

# Synthesis, structure and spectroscopic characteristics of $\text{Ti}(\text{O,C})_2$ /carbon nanostructured globules with visible light photocatalytic activity

V N KRASIL'NIKOV<sup>1</sup>, E V SHALAEVA<sup>1,\*</sup> , I V BAKLANOVA<sup>1</sup>, M A MELKOZEROVA<sup>1</sup>,  
M V KUZNETSOV<sup>1</sup>, E V ZABOLOTSKAYA<sup>1</sup>, O I GYRDASOVA<sup>1</sup>, L YU BULDAKOVA<sup>1</sup> and  
A M MURZAKAEV<sup>2</sup>

<sup>1</sup>Institute of Solid State Chemistry of the Ural Branch of the Russian Academy of Sciences,  
Ekaterinburg 620990, Russian Federation

<sup>2</sup>Institute of Electrophysics of the Ural Branch of the Russian Academy of Sciences,  
Ekaterinburg 620016, Russian Federation

MS received 29 April 2015; accepted 4 April 2016

**Abstract.** A morphology-controlled facile synthesis of titanium-glycolate precursors with subsequent annealing in He and air atmospheres has been exploited for the production of nanostructured composite globules, whiskers and plates of C-modified titanium dioxide. Characterisation tests proved the as-obtained globule composites to exclusively exhibit high-specific surface area (up to  $150\text{--}170\text{ m}^2\text{ g}^{-1}$ ), thus being useful for photocatalytic applications in the visible-light region. The combination of the electron paramagnetic resonance, X-ray photoelectron spectroscopy, absorption spectroscopy and transmission electron microscopy revealed the presence of three kinds of carbon in the globules: a small bandgap (with measured width of  $0.8\text{ eV}$ ) amorphous carbon surrounding the anatase nanocrystallites, C-containing radicals including carbonates on the surface of  $\text{TiO}_2$  and interstitial carbon in the oxygen position of the  $\text{TiO}_2$  lattice. It was found that the maximum visible-light photocatalytic activity of the globules is determined by the optimal surface concentration of amorphous carbon of about  $0.002\text{ wt.}\%\text{ m}^{-2}$ . Under these conditions, the highest synergic photosensitising effect on  $\text{TiO}_2$  nanocrystallites of all three kinds of carbon is expected.

**Keywords.** Carbon-modified titanium dioxide; synthesis; nanostructure; spectroscopy; optical and photocatalytic properties.

## 1. Introduction

Titanium dioxide is a promising photocatalyst for the decomposition of organic impurities in air and water, due to its high photoactivity, stability, non-toxicity and low-cost production [1–5]. Being a semiconductor with a bandwidth of  $3.0\text{--}3.2\text{ eV}$ , titanium dioxide in the form of rutile and anatase absorbs a relatively small amount of solar energy ( $4\text{--}5\%$ ) with a quantum yield lower than  $10\%$ . Numerous investigations have been carried out with the expectation of extending its absorption to the long-wave spectral region by producing carbon-modified  $\text{TiO}_2$  nanomaterials. Carbon doping of  $\text{TiO}_2$  in Ti- and O-lattice positions is known to introduce new energy levels in the bandgap, thus leading to optical bandgap narrowing. In addition, the interface between small bandgap carbon and  $\text{TiO}_2$  or the presence of active carbon-containing species (radicals) on the  $\text{TiO}_2$  surface was reported to improve its light absorption and electron transfer properties (photosensibilisation effect) [6]. All the above-mentioned effects promote the generation of electron–hole pairs under visible light as well as the production of reactive

oxidising species ( $\bullet\text{OH}$ ,  $\text{O}_2^-$ ,  $\bullet\text{OOH}$ ) on the catalyst surface, which can further lead to transformation of pollutants [7].

Carbon-modified  $\text{TiO}_2$  nanomaterials include C-activated  $\text{TiO}_2$  nanoparticles (nanorods, nanowires, nanograins, nanotubes) [8–12], nanostructured micro-aggregates or powders [13–20], as well as nanocarbon (nanotube, graphene, fullerene)- $\text{TiO}_2$  materials recently reviewed [6]. Nanostructured aggregates like titanium oxide-based spheres or globules have attracted interest as photocatalysts not only due to their large-specific surface area, but also because they display advantageous processing characteristics such as structural and mechanical stability, excellent reusable capability as well as block resistance [21–24].

Micro-aggregates and powders with a  $\text{TiO}_2/\text{C}$  composite structure are commonly synthesised either by the introduction of carbon particles into a  $\text{TiO}_2$  powder or a Ti-precursor sol (hydrothermal [13–16] and sol–gel [17] methods), or by the chemical vapour deposition of  $\text{TiO}_2$  on an activated carbon support [18]. Another synthesis approach involves one-step carbonisation of a self-assembled matrix containing Ti precursors and the intrinsic carbon source [19,20]. It should be mentioned that an advantage of the latter type of approaches can be the formation of both free carbon and other carbon states, such as interstitial carbon in the

\* Author for correspondence (shalaeva@ihim.uran.ru)

oxygen position of the  $\text{TiO}_2$  lattice as well as surface carbon-containing species (e.g., carbonates) capable of improving visible-light absorption [25,26].

Therefore, in an attempt to perform one-step carbonisation for producing nanostructured  $\text{TiO}_2/\text{C}$  composite aggregates, such as spheres or whiskers, one can exploit the carbonisation of mediate Ti-organic precursors prepared by morphology-controlled synthesis. It should be noted that a number of solvothermal and hydrothermal routes can be applied for the morphology-controlled synthesis of such precursor mediate micro-aggregates [27–30]. One-step carbonisation of mediate Ti-glycolate precursors has proven its efficiency, and we currently utilise it for the synthesis of composite aggregates with globule morphology and visible-light photocatalytic activity [31]. When considering these approaches, the first research objective is to understand how the synthesis conditions will affect the morphology of the as-prepared composite  $\text{TiO}_2/\text{C}$  aggregates, their specific surface area as well as the structure of globules comprising different carbon states. Here, along with the determination of the free carbon structure (amorphous, graphite nanocrystals or nanocarbons), which is known to affect its bandgap considerably [6,32,33], it is necessary to specify additional carbon states formed in the synthesised  $\text{TiO}_2/\text{C}$  composite globules. The second objective is an elucidation of the mechanism responsible for their photocatalytic activity, namely to study the relationship between the structural characteristics of the  $\text{TiO}_2/\text{C}$  composite globules and their optical and visible-light photocatalytic properties. It is particularly important to evaluate the bandgap in a free carbon component, because only nanoforms of carbon manifest themselves as small bandgap semiconductors [6]. However, for amorphous carbon, the width of the bandgap varies in a wide interval from 4.5 to 0.5 eV, depending on the  $sp^2$  cluster content (or spin concentration) [32–34].

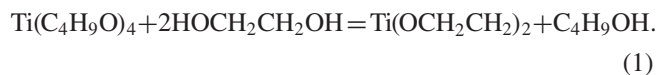
In this article, we further develop a two-stage synthesis for the production of  $\text{TiO}_2/\text{C}$  composites globules with visible-light photocatalytic activity and demonstrate how the synthesis conditions affect the morphology, specific surface area, structural and spectroscopic characteristics of the aggregates as well as the carbon chemical states in these composites. In a first stage, a morphology-controlled solvothermal route under altered titanium tetrabutoxide and ethylene glycol concentrations was employed for the synthesis of mediate Ti-glycolate precursors (a globule, a plate and a whisker). In a second stage, in order to optimise their structures and photocatalytic properties, the as-obtained precursors were subjected to one-step carbonisation by annealing initially in He and then in air atmospheres. A subsequent analysis showed that the globule composites exclusively demonstrate high-specific surface area (up to  $150\text{--}170\text{ m}^2\text{ g}^{-1}$ ) owing to their porous spherulitic structure and a shaggy surface, which is of importance for visible-light photocatalytic applications. Characterisation carried out by the transmission electron microscopy (TEM) and other spectroscopic methods (electron paramagnetic resonance (EPR), Raman, X-ray photoelectron and absorption spectroscopies) revealed three kinds of carbon in the synthesised globules: a small bandgap

( $E_g = 0.8\text{ eV}$ ) amorphous carbon surrounding the anatase nanocrystallites, C-containing radicals including carbonates in the near-surface layers of  $\text{TiO}_2$  as well as interstitial carbon in the oxygen position of the titanium dioxide lattice. It was found that the maximum visible-light photocatalytic activity of  $\text{Ti}(\text{O,C})_2/\text{C}$  composite globules is determined by an optimised surface concentration of amorphous carbon. When the latter is achieved, the highest synergic photosensitisation effect on  $\text{TiO}_2$  nanocrystallites of all three kinds of carbon is expected.

## 2. Experimental

### 2.1 Sample preparation

At the first stage, the  $\text{Ti}(\text{OCH}_2\text{CH}_2)_2$  glycolate precursor was synthesised using a solvothermal technique according to the below reaction:



For the synthesis of the precursor aggregates with different morphologies, titanium tetrabutoxide  $\text{Ti}(\text{C}_4\text{H}_9\text{O})_4$  and ethylene glycol  $\text{HOCH}_2\text{CH}_2\text{OH}$  reagents were taken in various volumetric ratios. The details of this solvothermal technique were described in our prior work [31].

The second stage involved a double-stepped isothermal annealing. To produce an intermediate carbon/titanium dioxide composite, the  $\text{Ti}(\text{OCH}_2\text{CH}_2)_2$  glycolate precursor was heated in a helium atmosphere at  $500^\circ\text{C}$  for 2 h. Then, in order to obtain a composite with an optimal ratio of carbon and titanium dioxide, the synthesised samples were annealed in air at 300, 325, 350, 375, 400, 450 and  $500^\circ\text{C}$ , with testing performed after each 2 h annealing stage.

### 2.2 Characterisation

The phase analysis of the samples was carried out by means of an X-ray powder diffractometer STADI-P (STOE) in  $\text{CuK}\alpha_1$  radiation using the PDF-2 X-ray diffraction database (Release 2009). The thermal analysis was performed on a Setsys Evolution thermal analyser (Setaram) in air atmosphere at a heating rate of  $5\text{ deg min}^{-1}$ . The carbon content in the synthesised samples was determined by using a METABAK-CS-10 gas analyser. The specific surface area of the samples was evaluated from the adsorption isotherms in accordance with the Brunauer–Emmett–Teller model (BET method).

The size and shape of the precursor aggregates and the products of their thermolysis were determined by the scanning electron microscopy (SEM) method using a MIRA3 TESCAN. The microstructures of the thermolysis products were investigated with the use of TEM using a JEM-200 CX and a JEM-2100. The samples were dispersed in an isobutyl alcohol bath by means of ultrasonic stirring followed by deposition of the sediments onto a copper microgrid coated with a thin holey carbon film.



Raman spectra were collected at room temperature using a RENISHAW-1000 spectrometer ( $\lambda = 633$  nm,  $P = 25$  mW). EPR spectra were recorded within the X-band (at a microwave frequency of 9.4 GHz) at room temperature on an Adany CMS-8400 EPR spectrometer. The concentration of

paramagnetic centres was derived from the integral intensity of EPR signal. High-purity CrCl<sub>3</sub> was used as the standard. The chemical compositions of the surface and valence states of carbon and oxygen in the samples were determined by X-ray photoelectron spectroscopy (XPS). The measurements

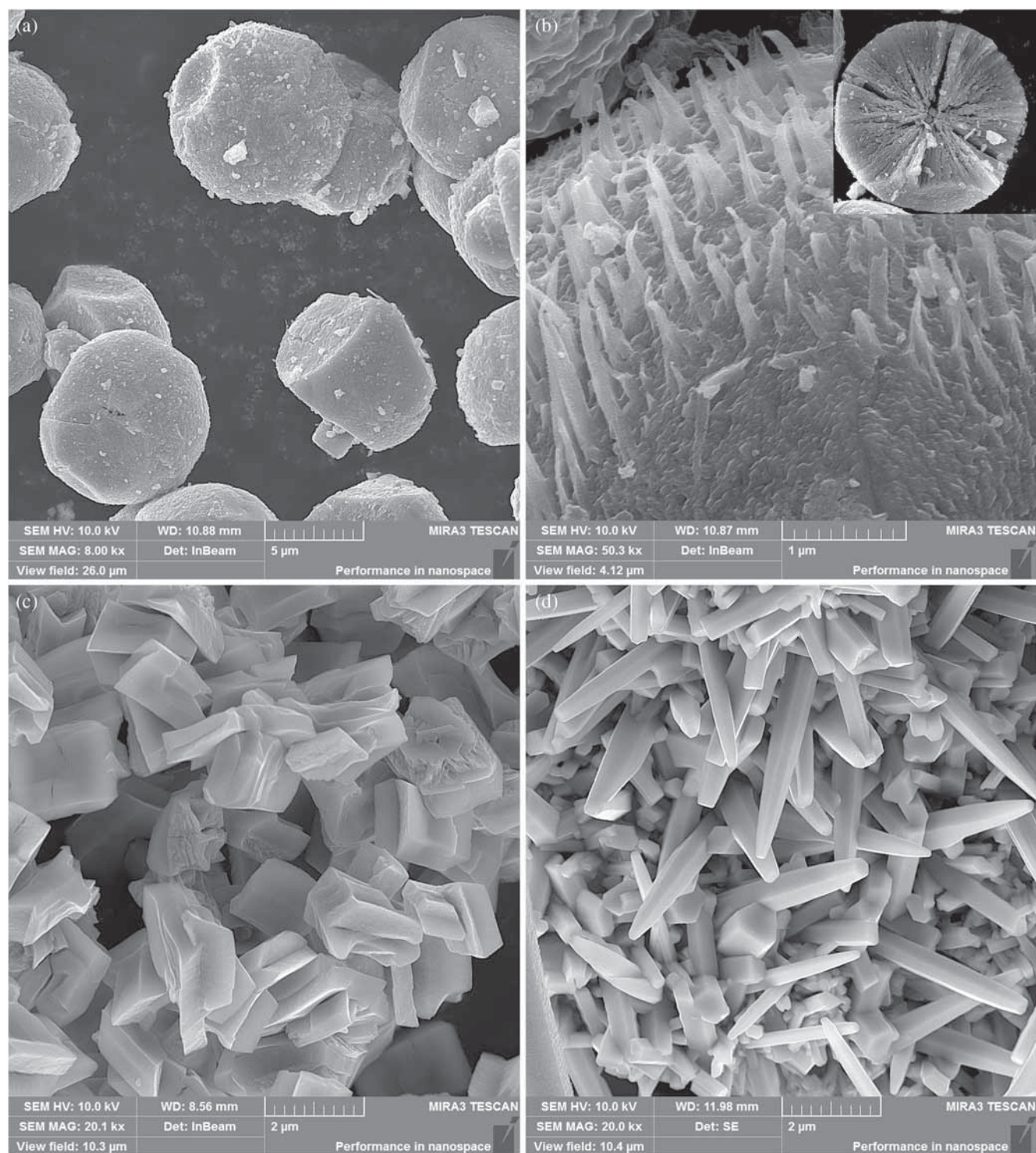


**Figure 1.** SEM images of titanium glycolate thermolysis products with various morphology: (a and b) globule; (c) plate; (d) whisker. Spherulitic structure and shaggy surface with nanosized whiskers (inset) are shown for globules (b). Thermolysis conditions: He atmosphere, 500°C.

were carried out using an ESCALAB MK spectrometer with nonmonochromatic  $\text{MgK}\alpha$  radiation (1253.6 eV). In the course of the XPS experiment, the residual pressure was maintained at a level of  $10^{-8}$  Pa.

Absorption spectra in the range of 190–800 nm were recorded with a UV-2401 PC spectrometer (Shimadzu,  $\lambda = 380$  nm).  $\text{BaSO}_4$  was used as the standard.

### 2.3 Photocatalytic activity test

The photocatalytic activity of the synthesised samples was estimated from the oxidation reaction of hydroquinone in water. The hydroquinone solutions with a concentration of  $4 \times 10^{-4} \text{ mol l}^{-1}$  and a total volume of 20 ml were subjected to irradiation in the visible spectral region using a 18 W luminescent lamp ( $\lambda_{\text{max}} = 425$  nm) under a 1-h exposure. A variation in the hydroquinone concentration was estimated using the voltammetric method. The photocatalyst mass was constant and amounted to 30 mg. In order to evaluate the stability of the samples during photocatalysis, the cycle of bringing one and the same catalyst into contact with the solution was repeated three times. The method of conducting the photocatalysis experiment is described in detail elsewhere [31,35].

## 3. Results and discussion

### 3.1 Intermediate C-modified $\text{TiO}_2$ aggregates synthesised by thermolysis in inert atmosphere from titanium glycolates with controllable morphology

Ti-glycolate precursor aggregates synthesised by reaction (1) reveal different morphologies depending on the volumetric ratio of titanium tetrabutoxide  $\text{Ti}(\text{C}_4\text{H}_9\text{O})_4$  and ethylene glycol  $\text{HOCH}_2\text{CH}_2\text{OH}$ . Under increased solvent (ethylene glycol) and decreased Ti-glycolate concentrations, the aggregate morphology of such a precursor undergoes a change from a globule (ratio: 1/2–1/10) to a plate and then to a whisker (ratio: 1/10–1/50). Low solvent concentrations and high Ti-glycolate supersaturation lead to rapid crystallisation producing globule morphology Ti-glycolates. Figure 1 presents the SEM images of the samples with different aggregate morphologies produced by heating of glycolate precursors in inert atmosphere at 500°C. As is typical of the precursor technology [27–30], the aggregates of thermolysis products inherit the morphology of the precursor crystals. The SEM study of the globule fracture displays signs of the spherulitic porous structure, as shown in figure 1b (inset), which can be expected for globules growing under conditions of high supersaturation [36]. Furthermore, the SEM images of the globule aggregates presented in figure 1b reveal porous and shaggy surfaces with longitudinal nanosized whiskers.

According to the results of X-ray (figure 2) and elemental analysis, all the thermolysis products of a  $\text{Ti}(\text{OCH}_2\text{CH}_2)_2$  glycolate in an inert atmosphere include the anatase phase of titanium dioxide and contain 16–21 wt.% carbon, the

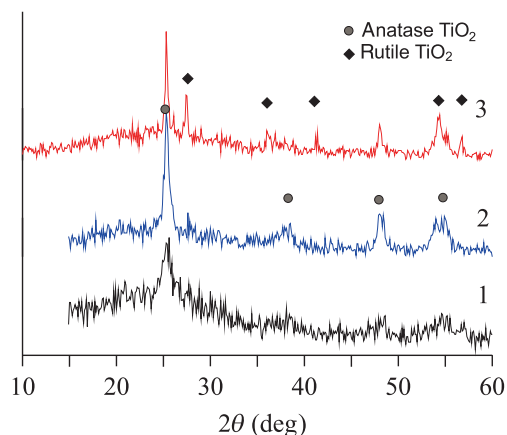


**Figure 2.** XRD spectra for the samples prepared by thermolysis in He atmosphere at 500°C (1), and by double-stepped annealing of a precursor in He atmosphere and then in air atmosphere at 450°C (2), 500°C (3).

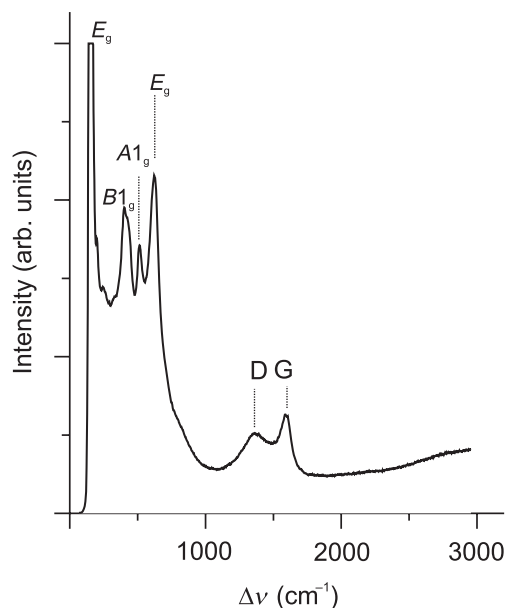


**Figure 3.** The Raman spectrum of thermolysis product with globule morphology. Thermolysis conditions: He atmosphere, 500°C. The lines of  $\text{TiO}_2$ -anatase ( $E_g$ ,  $B1_g$ ,  $A1_g$ ) and free carbon (D and G) are identified.

concentration of which increases under increased solvent (ethylene glycol) concentration. The presence of free carbon in the thermolysis products is confirmed both by the elemental analysis and Raman spectroscopy data displayed in figure 3. Along with the lines belonging to the vibrational spectrum of anatase ( $147 \text{ cm}^{-1}$  ( $E_g$ ),  $397 \text{ cm}^{-1}$  ( $B1_g$ ),  $513 \text{ cm}^{-1}$  ( $A1_g$ ) and  $633 \text{ cm}^{-1}$  ( $E_g$ )), the Raman spectra of the samples exhibit two rather intensive lines typical of free carbon (D band at  $1357 \text{ cm}^{-1}$  and G band at  $1599 \text{ cm}^{-1}$ ). These lines may be attributed to hydrogenated amorphous carbon, which is likely to form under annealing of an organic precursor in He [37].



TEM makes it possible to determine the internal structure of the thermolysis products of titanium glycolate. A typical selected area electron diffraction pattern taken from the globule or whisker area is shown in figure 4a. It contains Debye rings with a homogeneous distribution of intensity, which are identified by the anatase structure of titanium oxide and testify to the nanocrystalline state of this phase. As follows from the Debye ring intensity distribution, the particle size does not exceed 20 nm. The bright-field electron microscopy images of the thermolysis products exhibit a diffraction contrast typical of the amorphous-crystalline state, which is evidenced in figure 4b. As can be seen in figure 5a, the high-resolution transmission electron microscopy image confirms the amorphous-crystalline structure of the thermolysis products. Nanocrystalline graphite and nanocarbons such as nanotubes or fullerenes were not revealed. Thus, all the products obtained by the thermolysis of titanium glycolate in inert atmosphere mostly comprise of titanium dioxide/carbon composites having an amorphous-crystalline structure. The nanosized crystallites of the anatase phase are surrounded by an amorphous carbon matrix. A similar amorphous-nanocrystalline structure promotes an increase in the specific surface area, in addition to porosity. The composite structure of the thermolysis products is retained when the annealing temperature in inert atmosphere is increased up to 900°C. Characterisation tests showed that the globule

composites exclusively demonstrate high-specific surface areas due to their porous spherulitic structure and a shaggy surface, which is of relevance for catalytic applications.

In order to optimise the structure of the globule composites, their chemical composition and free carbon content, an additional thermal treatment in air was carried out producing aggregates with improved photocatalytic activity in visible light [31]. Here, in an attempt to elucidate the mechanism responsible for their photocatalytic activity and to characterise amorphous carbon and other chemical states of carbon, including interstitial carbon in TiO<sub>2</sub> lattice, we performed EPR and XPS spectroscopic investigations in globule aggregates.

### 3.2 Ti(O,C)<sub>2</sub>/C composite nanostructured globules prepared by adjustable annealing in air: structural properties and spectroscopic data (Raman, EPR and XPS methods)

The intermediate titanium dioxide/carbon globules prepared by thermolysis in inert atmosphere described above were then annealed in air at 300, 325, 350, 375, 400, 450 and 500°C.

The Raman spectra of the globule samples exhibited an abrupt decrease in the intensity of characteristic lines (D and G) of free carbon with an increase in the annealing temperature. Following annealing at 375°C, the spectral lines were

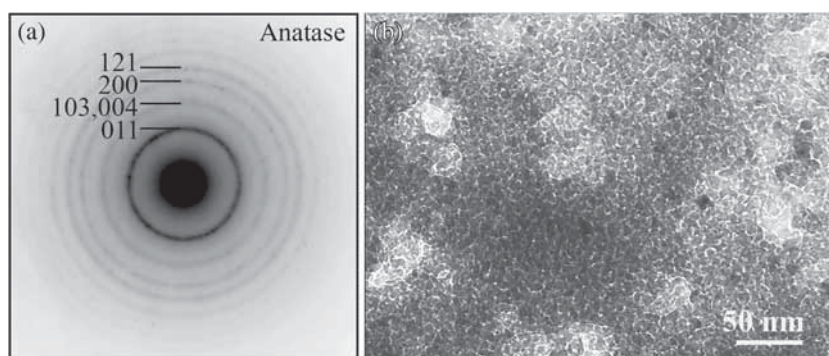


**Figure 4.** (a) Selected area electron diffraction pattern and (b) bright field TEM image taken for typical globule area with amorphous-nanocrystalline structure.

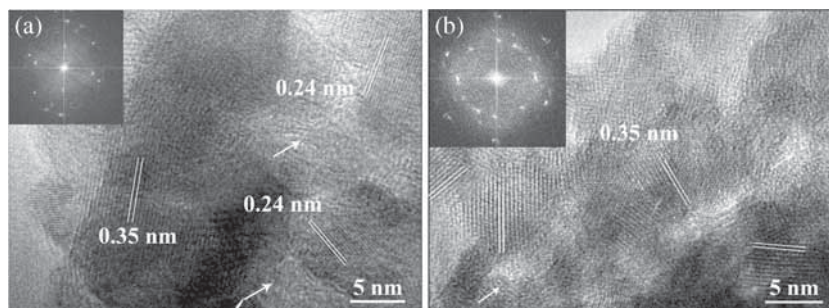


**Figure 5.** High-resolution transmission electron microscopy images of areas of titanium dioxide/carbon amorphous-nanocrystalline globules prepared by (a) annealing of a precursor in He atmosphere and (b) by double-stepped annealing in He and then in air atmospheres at 375°C. Amorphous phase zones are shown by arrows.

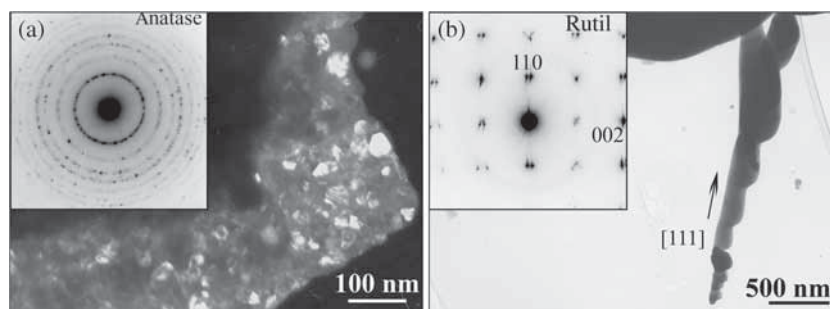


**Figure 6.** Microstructure of titanium dioxide/carbon globules prepared by double-stepped annealing in He and then in air atmospheres at 375°C: (a) dark field TEM image of anatase crystallites and SAED (inset); (b) bright field TEM image of the whisker with signs of oriented growth of rutile crystallites and SAED (inset).

completely suppressed, which agrees well with the elemental and thermogravimetric analysis data. However, the TEM image in figure 5b clearly reveals the amorphous-crystalline state in the samples annealed at 300°C as well as at 375°C. In some exceptional cases, an increase in the sizes of anatase crystallites was observed, as shown in figure 6a. The anatase modification remains primary; however, rutile crystallites appear only in the longitudinal nanosized whiskers revealing signs of oriented growth under annealing at 375°C (figure 6b). According to XRD spectra (figure 2), the rutile formation starts at the annealing temperatures above 450°C. Globules prepared by annealing in air at 325–350°C demonstrated high-specific surface area ( $S$ ), with  $S$  varying from 174 to 148 m<sup>2</sup> g<sup>-1</sup>. When the annealing temperature reached 450°C, the specific surface area gradually decreased to 49 m<sup>2</sup> g<sup>-1</sup>. Here, it should be noted that nanostructured whisker composites annealed at 300°C showed a low-specific surface area of less than 30 m<sup>2</sup> g<sup>-1</sup>.

More detailed information on the presence of the amorphous carbon and carbon-containing clusters and radicals, as well as the data on spin concentration in amorphous carbon, were obtained by EPR spectroscopy. Figure 7 shows the EPR spectra of the samples subjected to double-stepped annealing (first in He atmosphere and then in air) as well as the spectrum of the samples annealed solely in He atmosphere. The characteristics of the EPR spectra for various samples are presented in table 1.

For the samples annealed solely in He atmosphere, we observed the narrow, high-intensity EPR signal presented in figure 7a, which can be precisely simulated with a single Lorentzian component with a  $g$ -factor of 2.0032 and a peak-to-peak line width of  $\Delta H = 3.08$  G. A similar EPR spectrum was recorded for a carbon matrix prepared from composite samples boiled in hydrofluoric acid to dissolve the titanium dioxide. A minor increase in the  $g$ -factor (2.0041) and a slightly broadened Lorentzian component ( $\Delta H = 3.22$  G) are characteristic of such an EPR signal. These data point to the fact that the EPR signals for the samples annealed both in the He and air atmospheres belong to the paramagnetic centres typical of amorphous carbon. The  $g$ -factor for polymer- and diamond-like amorphous carbon films is commonly

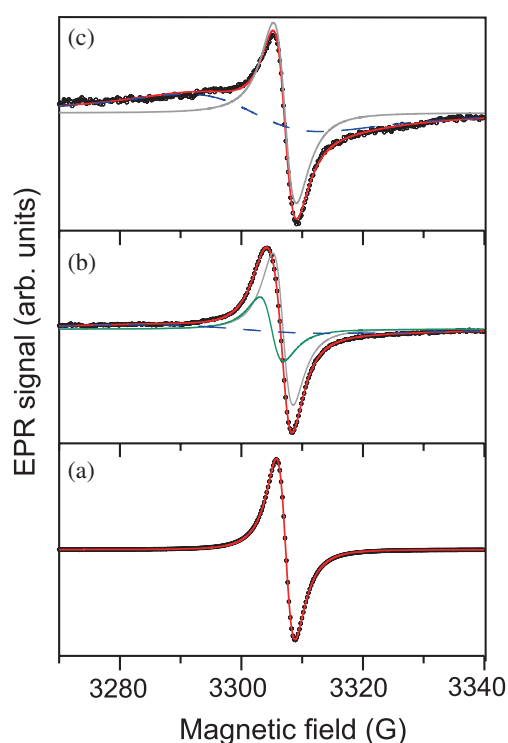


**Figure 7.** EPR spectra of titanium dioxide/carbon globules: (a) prepared by annealing of a precursor in He atmosphere at 500°C; (b) and (c) prepared by double-stepped annealing of a precursor in He and then in air at 350 and 400°C, respectively. The spectra were recorded at room temperature. In all cases, open circles represent the experimental data, solid red lines is a fit, while coloured dash and grey solid lines display individual Lorentzian components.

varied within a range of 2.0028 and 2.0045, depending on the environment and preparatory conditions [32,33,38,39]. It is assumed that the variations in both the  $g$ -factors and the linewidth of the EPR signal in amorphous carbon are promoted by changing the content and size of the sp<sup>2</sup> clusters that predominantly provide the paramagnetic centres. The measured spin concentration in a sample annealed in a He atmosphere is equal to  $2 \times 10^{18}$  spin g<sup>-1</sup>; in this case, the spin concentration for carbon in these samples is about

**Table 1.** Parameters of EPR lines for globules treated by annealing in He at 500°C (1) and by two-stepped annealing in He (500°C) and then in air atmospheres (2) at various temperatures.

Preparing conditions	$I_1$	$\Delta H_1$	$g_1$	$I_2$	$\Delta H_2$	$g_2$
(1)	533933	3.08	2.0032	—	—	—
(2), 300°C	15345	3.95	2.0033	—	—	—
(2), 325°C	4429	4.16	2.0038	78	32.5	2.0077
(2), 350°C	1343	4.16	2.0034	63	31	2.0075
(2), 375°C	920	4.02	2.0033	69	29.3	2.0070
(2), 400°C	428	3.98	2.0031	86	22.5	2.0058
(2), 450°C	20	3.64	2.0027	2	22.1	2.0056
Carbon matrix prepared from composite (2)	—	3.22	2.0041	—	—	—

$10^{19}$  spin  $g^{-1}$ . Therefore, according to the correlations between the spin concentration, linewidth of EPR signal and optical bandgap, which were determined for amorphous carbon films [32], amorphous carbon in composite globules can be expected to behave as a small bandgap semiconductor with an optical gap of less than 2 eV.

After annealing the samples in air, the above-mentioned narrow EPR line with a  $g$ -factor of  $2.0034 \pm 0.0004$  becomes slightly asymmetrical; this is known to be an intrinsic feature of the behaviour of amorphous carbon under thermal treatment. This effect is more pronounced for samples annealed at 350°C, as represented in figure 7b. Figure 8 presents the dependency of the annealing temperature on the intensity of the EPR spectrum line, due to the paramagnetic centres in amorphous carbon whose content decreases with temperature. The measured concentration of paramagnetic centres in the sample annealed at 300°C in air was equal to  $1 \times 10^{17}$  spin  $g^{-1}$ , whereas the spin concentration in carbon was seen to decrease slightly to  $0.2 \times 10^{19}$  spin  $g^{-1}$ . When the intensity of the EPR signal is significantly reduced ( $T_{an} \geq 325^\circ\text{C}$ ), the spectra of the samples reveal a weak, broad Lorentzian line with a  $g$ -factor of  $2.007 \pm 0.007$  and a linewidth of  $\Delta H \approx 29$  G in addition to the narrow line having a  $g$ -factor of 2.0034 and a linewidth of  $\Delta H = 4.05 \pm 0.1$  G, as presented in figure 7b and c. The intensity of this signal is approximately constant with annealing temperature. Thus, the broadened EPR component can be associated with the paramagnetic carbon clusters or carbon-containing radicals (for example,  $\text{CO}_2^-$  [40,41]) attendant on the near-surface layer of titanium dioxide. Both narrow and broad EPR signals were observed up to 450°C. Hence, the surfaces of samples annealed at temperatures of 400 and 450°C are certain to feature remnant carbon-containing radicals and carbon clusters.

Therefore, the EPR spectroscopy study demonstrated that nanostructured  $\text{TiO}_2$ -based globules treated by adjustable annealing in air comprise amorphous carbon as well as C-containing surface radicals and clusters at annealing temperatures of up to 450°C. The presence of paramagnetic carbon centres related to the interstitial carbon in the oxygen sites

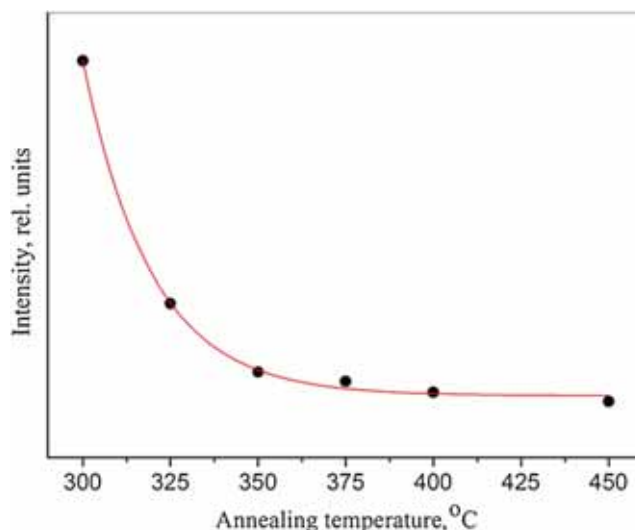


**Figure 8.** Intensity of the free carbon EPR signal ( $g = 2.0034$ ) in terms of the air annealing temperature for titanium dioxide/carbon globules.

of the  $\text{TiO}_2$  lattice cannot be excluded. *Ab initio* calculations show either paramagnetic or non-paramagnetic properties of these defects depending on the site (Ti-position, O-position, C–O surface binding) [42,43]. For these samples, we did not manage to detect a characteristic EPR signal of  $(\text{O}_2)^-$  radicals and  $\text{Ti}^{3+}$  centres, both of which are known to appear due to the oxygen vacancy in titanium dioxide [40,44].

XPS spectroscopy was carried out to investigate the chemical state of carbon in the surface layers of  $\text{TiO}_2$  and to clarify whether carbon atoms occupy the interstitial site of the  $\text{TiO}_2$  lattice in the composites synthesised by double-stepped annealing (in He and in air) from Ti-glycolate precursors. Figure 9 displays the survey and C1s core-level spectra for a sample treated by a double-stepped annealing process, with an annealing temperature in air of 350°C. The C1s core-level spectrum can be easily decomposed into three peaks with binding energies of 284.6, 286.4 and 288.7 eV. The most intensive peak at a low-binding energy (284.6 eV) can be assigned to the characteristic C1s peak of amorphous carbon, for which the  $\text{sp}^2/\text{sp}^3$  hybridisation ratio is close to 1 [45]. The peaks at 286.4 and 288.7 eV are commonly attributed to the presence of carbonate groups C–O, C=O, O–C=O and C–OR(H), which are observed for  $\text{TiO}_2$ –C samples synthesised from precursors containing different molecular carbon species [25,26,41,46]. The carbonate and hydrocarbonate surface species are removed by Ar-ion etching (4 keV, current of 20  $\mu\text{A}$ ), with the weak peak at 282.2 eV being resolved within the C1s core-level spectrum in addition to a peak assigned to amorphous carbon. The revealed weak peak can be attributed to a Ti–C bond, testifying to the fact that carbon occupies the O-site in the  $\text{TiO}_2$  lattice [47]. This peak was not detected for the samples that were prepared by annealing at temperatures above 400°C; this may be due to a considerable decrease in the concentration of interstitial carbon with temperature.

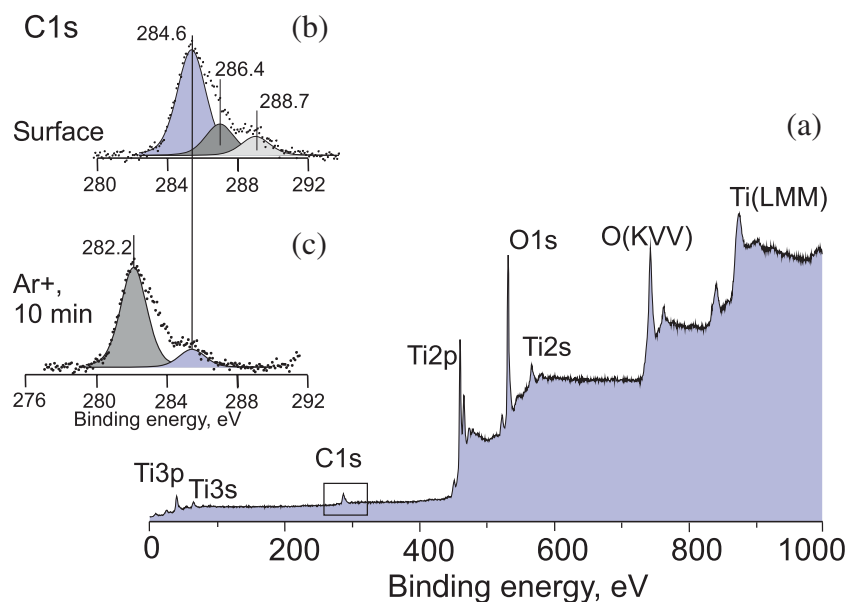


**Figure 9.** XPS spectra for  $\text{Ti}(\text{O,C})_2/\text{carbon}$  globules prepared by double-stepped annealing of precursor in He and then in air at  $350^\circ\text{C}$ : (a) survey; (b)  $\text{C1s}$  core level, surface; and (c)  $\text{C1s}$  core level,  $\text{Ar}^+$  ion etching.

Thus, it has been found that the globules prepared by one-step carbonisation (annealing of a Ti-organic precursor first in inert and then in air atmospheres) are nanostructured composites characterised by a high-specific surface area ( $174\text{--}50\text{ m}^2\text{ g}^{-1}$ ) under an annealing temperature of up to  $450^\circ\text{C}$ .  $\text{TiO}_2$  nanocrystallites were shown to be partially or fully surrounded by amorphous carbon and to exhibit C-containing radicals including carbonates in the near-surface layers of  $\text{TiO}_2$ . Carbon interstitial atoms in the  $\text{TiO}_2$  lattice were additionally detected by XPS study for the synthesised globules. Based on the data on the spin concentration and width of an EPR signal, the amorphous carbon can be considered as a small bandgap semiconductor with an optical gap of less than 2 eV.

### 3.3 Optical and photocatalytic properties of $\text{Ti}(\text{O,C})_2/\text{C}$ composite nanostructured microglobules

In this section, we will analyse the data on optical absorption of the globule composites and a carbon matrix prepared from the composites using information on the carbon chemical states obtained by EPR and XPS spectroscopies. Figure 10a demonstrates absorption spectra in the visible and ultraviolet regions for  $\text{Ti}(\text{O,C})_2/\text{C}$  microglobules prepared both by annealing solely in He atmosphere and by double-stepped annealing (in He and then in air atmospheres) at various temperatures. The absorption spectrum of the sample not subjected to air annealing coincides completely with that of a carbon matrix prepared from the  $\text{Ti}(\text{O,C})_2/\text{C}$  composite microglobules. According to Tauc equation [48] and the absorption experiment performed for an amorphous carbon matrix prepared from the  $\text{C}/\text{TiO}_2$  samples under consideration (figure 11), this carbon reveals a direct bandgap ( $E_g$ ) of

0.8 eV, which is consistent with the characteristics of small bandgap amorphous carbon [32–34]. For the air-annealed  $\text{Ti}(\text{O,C})_2/\text{C}$  composites, an abrupt decrease in absorption, which is typical of titanium dioxide (in vicinity of 3 eV), markedly shifts towards the visible-light region owing to the absorption contribution of amorphous carbon, as can be seen in figure 10b. Under increased annealing temperature (from 300 up to  $400^\circ\text{C}$ ) and decreased amorphous carbon contribution, the optical bandgap of modified  $\text{TiO}_2$  may be evaluated to rise from 2.1 to 3.1 eV, thus approaching the optical bandgap of unmodified  $\text{TiO}_2$  ( $E_g = 3.2$  eV). On the other hand, annealing at higher temperatures of 450 and  $500^\circ\text{C}$  results in optical bandgap narrowing ( $E_g = 2.9$  and 2.85 eV, respectively). At these temperatures, a large amount of  $\text{TiO}_2$  undergoes the anatase-rutile phase transformation (figure 2), with the observed optical gap being lower than that of the non-modified rutile ( $E_g = 3.0$  eV).

Thus, based on the absorption spectra and EPR data regarding the content of amorphous carbon clusters, it can be concluded that the small bandgap amorphous carbon layers covering  $\text{TiO}_2$  do enhance the absorption in the visible region for those samples prepared by a double-stepped annealing at  $300\text{--}450^\circ\text{C}$ . C-containing radicals and other species, e.g., carbonates, detected by EPR and XPS on the dioxide titanium surface can act as photosensitisers. In addition, interstitial carbon in the oxygen site of the  $\text{TiO}_2$  lattice observed by XPS can be responsible for a slight shift of the absorption band edge towards the visible-light region. Therefore, in accordance with the photocatalysis mechanism [6,25], the enhanced photoabsorption in the visible region could have intensified the generation of electron-hole pairs in  $\text{Ti}(\text{O,C})_2$  and enhanced electron transfer towards the conduction band of titanium dioxide owing to coupling of  $\text{TiO}_2$



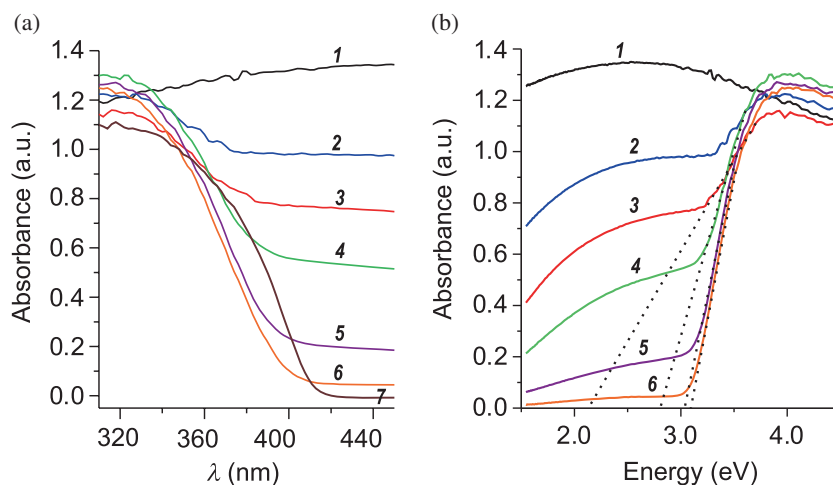


**Figure 10.** Ultraviolet–visible absorption ( $\alpha$ ) spectrum in terms of (a) wavelength and (b) photon energy for Ti(O,C)<sub>2</sub>/carbon globules prepared by annealing of precursor in He atmosphere (1) and by double-stepped annealing in He and then in air at temperatures 250 (2), 300 (3), 325 (4), 350 (5), 400 (6) and 500°C (7). The ultraviolet–visible absorption spectrum for the carbon matrix obtained from the composite coincides with the absorption spectrum for globules (1).

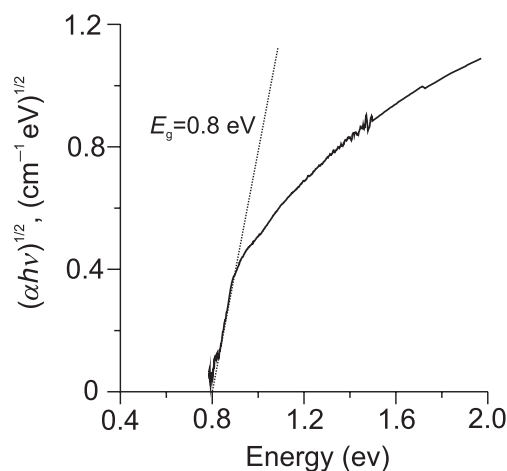


**Figure 11.** Photon energy ( $h\nu$ ) dependence of  $(\alpha h\nu)^{1/2}$  and evaluation of the optical gap ( $E_g$ ) for amorphous carbon matrix prepared from Ti(O,C)<sub>2</sub>/carbon globules.

with small bandgap amorphous carbon and C-containing surface species. As a result, this could have been responsible for promoting the production of reactive oxidising species ( $\bullet\text{OH}$ ,  $\text{O}_2^-$ ,  $\bullet\text{OOH}$ ) on the titanium oxide surface under visible light.

The photocatalytic activity of the synthesised Ti(O,C)<sub>2</sub>/C composite globules was studied by the oxidation reactions of aqueous solutions of hydroquinone in the visible spectral region [31]. The dependences of the hydroquinone oxidation rate constant for the photocatalysts produced by annealing in the temperature range from 250 to 500°C are presented in figure 12. All Ti(O,C)<sub>2</sub>/C samples were shown to be photocatalytically active in visible light unlike pristine TiO<sub>2</sub> and the commercial photocatalyst Degussa P25, which are completely inactive in this light range. The dependence of

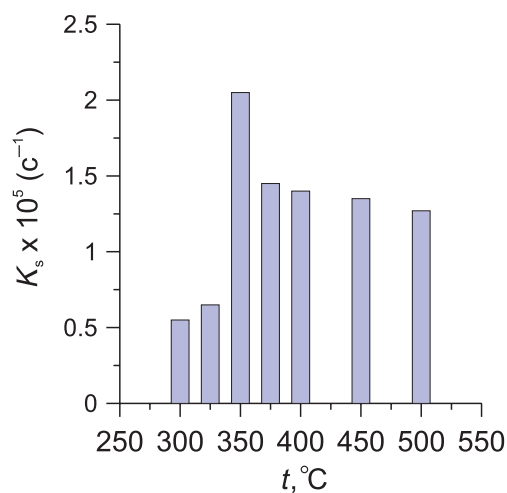


**Figure 12.** The dependence of the oxidation rate constant of hydroquinone with catalysts based on Ti(O,C)<sub>2</sub>/carbon globules in terms of air annealing temperature.

photocatalytic activity on the annealing temperature is a nonmonotonic function. The maximum oxidation rate was observed for the samples annealed at 350°C. Upon a further increase in the annealing temperature and a decrease in all kinds of carbon and specific surface area, the hydroquinone oxidation rate declined exponentially. The samples prepared at temperatures below 350°C demonstrated a minimum reaction rate. Since these samples exhibit the highest specific surface area and maximum magnitudes of photoabsorption compared with other samples, such behaviour is most likely related to the excess of amorphous carbon whose surface concentration is the largest (0.0086 wt.% m<sup>-2</sup>). The excess of amorphous carbon does not produce an efficient photosensibilisation effect on TiO<sub>2</sub>; moreover, it shields the surface

centres of C-modified TiO<sub>2</sub> thus decelerating the production of reactive oxidising species ( $\bullet\text{OH}$ ,  $\text{O}_2^-$ ,  $\bullet\text{OOH}$ ) on the catalyst surface. Therefore, the enhanced photocatalytic activity of Ti(O,C)<sub>2</sub>/C composite globules synthesised at 350°C is determined by an optimised carbon content (including that of amorphous carbon equal to 0.002 wt.% m<sup>-2</sup>), which provides a more noticeable photosensitisation effect on TiO<sub>2</sub> owing to all three kinds of carbon detected in the samples (small bandgap amorphous carbon; C-containing surface species, such as carbonates; and interstitial C in the oxygen position in TiO<sub>2</sub>) and a minimal shielding of the surface reactive centres of titanium dioxide.

#### 4. Conclusion

A two-stage morphology-controlled facile approach has been applied for the synthesis of nanostructured titanium dioxide/carbon composites with a globular morphology of microaggregates and enhanced visible-light photocatalytic activity. At first, a morphology-controlled solvothermal route under altered titanium tetrabutoxide and ethylene glycole concentrations was employed for the synthesis of mediate Ti-glycolate precursors (microglobules, microplates and microwhiskers). Then, the as-obtained microglobule precursors were subjected to one-step carbonisation by annealing in He and then in air atmospheres at temperatures of 300–450°C.

All synthesised microaggregates prepared by one-step carbonisation were found to be nanostructured composites, with TiO<sub>2</sub> nanocrystallites being partially or fully surrounded by amorphous carbon. Globule aggregates demonstrated a spherulitic porous structure, a shaggy surface and a high-specific surface area (174–50 m<sup>2</sup> g<sup>-1</sup>). However, the aggregates exhibiting other morphology types (a whisker or a plate) demonstrated a low-specific surface area (less than 30 m<sup>2</sup> g<sup>-1</sup>), which is not advantageous for photocatalysis applications. For globule composites, the combination of the EPR and XPS methods revealed the presence of amorphous carbon clusters and C-containing radicals, including carbonates, in the near-surface layers of TiO<sub>2</sub> at an annealing temperature of up to 450°C. In addition, the XPS study detected interstitial carbon in the oxygen position of the titanium dioxide lattice.

The enhanced visible-light absorption of the synthesised Ti(O,C)<sub>2</sub>/C composite microglobules was found to be mostly due to a small bandgap of amorphous carbon matrix with a measured optical band of 0.8 eV. C-containing surface radicals, such as carbonates and interstitial carbon detected in composites, are supposed to improve the visible-light absorption of the Ti(O,C)<sub>2</sub>/C composites.

It has been found that the maximum visible-light photocatalytic activity of Ti(O,C)<sub>2</sub>/C microglobules is determined by the optimal surface concentration of amorphous carbon of about 0.002 wt.% m<sup>-2</sup>, in which case the highest synergic photosensitizing effect on TiO<sub>2</sub> nanocrystallites of all three kinds of carbon (small bandgap amorphous

carbon, C-containing surface species, such as carbonates, and interstitial C in the oxygen-position in TiO<sub>2</sub>) is expected.

#### Acknowledgements

We are grateful to N G Popova, the Foreign Languages Department of the Institute of Law and Philosophy, the Ural Branch of RAS, for the help in preparing the English version of the manuscript. This work was supported by the Russian Foundation for Basic Research (grant no. 13-03-00265-a).

#### References

- [1] Hashimoto K, Irie H and Fugishima A 2005 *Japn. J. Appl. Phys.* **44** 8269
- [2] Zaleska 2008 *Recent Patents on Engineering* **2** 157
- [3] Yu H, Irie H and Hashimoto K 2010 *J. Am. Chem. Soc.* **132** 6898
- [4] Hsiao Y C, Wu T F, Wang Y C, Hu C C and Huang C 2014 *Appl. Catal. B: Environ.* **148–149** 250
- [5] Lazar M A, Varghese S and Nair S S 2012 *Catalysis* **2** 572
- [6] Leary R and Westwood A 2011 *Carbon* **49** 741
- [7] Pelaez M, Nolan N T, Pillai S C, Seery M K, Falaras P, Kontos A G et al 2012 *Appl. Catal. B: Environ.* **125** 331
- [8] Reddy K M, Baruwati B, Jayalakshmi M, Rao M M and Manorama S V 2005 *J. Solid State Chem.* **178** 3352
- [9] Wang Y, Huang Y, Ho W, Zhang L, Zou Z and Lee S 2009 *J. Hazard. Mater.* **169** 77
- [10] Zhong J, Chen F and Zhang J L 2010 *J. Phys. Chem. C* **114** 933
- [11] Liu Y, Liu X, Lu D, Fang P, Xiong R, Wie J and Pan C 2014 *J. Mol. Catal. A: Chem.* **392** 208
- [12] Wu Z B, Dong F, Zhao W R, Wang H Q, Liu Y and Guan B H 2009 *Nanotechnology* **20** 235701
- [13] Ren W J, Ai Z H, Jia F L, Zhang L Z, Fan X X and Zou Z G 2007 *Appl. Catal. B: Environ.* **69** 138
- [14] Wu X, Yin S, Dong Q and Sato T 2014 *Appl. Catal. B: Environ.* **156–157** 257
- [15] Wang X, Hu Z, Chen Y, Zhao G, Liu Y and Wen Z 2009 *Appl. Surf. Sci.* **255** 3953
- [16] Asilturk M and Sener S 2012 *Chem. Eng. J.* **180** 354
- [17] Tryba B, Morawski A W and Inagaki M 2003 *Appl. Catal. B: Environ.* **41** 427
- [18] Gianluca L P, Bono A, Krishnaiah D and Collin J G 2008 *J. Hazard. Mater.* **157** 209
- [19] Stefik M, Lee J and Wiesner U 2009 *Chem. Commun.* **18** 2532
- [20] Lee Y F, Chang K H, Hu C C and Lin K M 2010 *J. Mater. Chem.* **20** 5682
- [21] Tang G, Liu S, Tang H, Zhang D, Li C and Yang X 2013 *Ceram. Intern.* **39** 4969
- [22] Du J, Chen W, Zhang C, Liu Y, Zhao C and Dai Y 2011 *Chem. Eng. J.* **170** 53
- [23] Ma Y, Ji G, Ding B and Lee J Y 2012 *J. Mater. Chem.* **22** 24380
- [24] Zhang B, Chen B, Shi K, He S, Liu X, Du Z et al 2003 *Appl. Catal. B: Environ.* **40** 253
- [25] Chen D, Jiang Z, Geng J, Wang Q and Yang D 2007 *Ind. Eng. Chem. Res.* **46** 2741

- [26] Park Y, Kim W, Park H, Tachikawa T, Majima T and Choi W 2009 *Appl. Catal. B: Environ.* **91** 355
- [27] Wang D, Yu R, Chen Y, Kumada N, Kinomura N and Takano M 2004 *Solid State Ionics* **172** 101
- [28] Zhong L S, Hu J S, Wan L J and Song W G 2008 *Chem. Commun.* **10** 1184
- [29] Krasil'nikov V N, Shtin A P, Gyrdasova O I, Polyakov E V and Shveikin G P 2008 *Russ. J. Inorg. Chem.* **53** 1065
- [30] Dong S, Chen X, Gu L, Zhou X, Xu H, Wang H *et al* 2011 *Appl. Mater. Interfaces* **3** 93
- [31] Krasil'nikov V N, Zhukov V P, Baklanova I V, Gyrdasova O I and Buldakova L Yu 2015 *Catal. Lett.* **145** 1290
- [32] Barklie R C 2010 *Diam. Relat. Mater.* **10** 174
- [33] Ristein J, Schafer J and Ley L 1995 *Diam. Relat. Mater.* **4** 508
- [34] Tamor M A, Haire J A, Wu C H and Hass K C 1989 *Appl. Phys. Lett.* **54** 123
- [35] Krasil'nikov V N, Shtin A P, Gyrdasova O I, Polyakov E V, Buldakova L Yu, Yanchenko M Yu *et al* 2010 *Russ. J. Inorg. Chem.* **55** 1184
- [36] Shubnikov A V and Sheftal N N 1966 *Growth of crystals* (New York: Consultants Bureau)
- [37] Ferrari A C and Robertson J 2001 *Phys. Rev. B* **64** 075414
- [38] Kausteklis J, Cevc P, Arcon D, Nasi L, Pontiroli D, Mazzani M and Ricco M 2011 *Phys. Rev. B* **84** 125406
- [39] Bardeleben H J, Cantin J L, Zellama K and Zeinert A 2003 *Diam. Relat. Mater.* **12** 124
- [40] Konstantinova E A, Kokorin A I, Sakthivel S, Kisch H and Lips K 2007 *Chimia* **61** 810
- [41] Liu G, Han C, Pelaez M, Zhu D, Liao S, Likodimos V *et al* 2012 *Nanotechnology* **23** 294003
- [42] Yang K, Dai Y, Huang B and Whangbo M H 2009 *J. Phys. Chem. C* **113** 2624
- [43] Zaynullina V, Zhukov V, Krasil'nikov V, Yanchenko M, Buldakova L and Polyakov E 2010 *Phys. Solid State* **52** 271
- [44] Green J, Carter E and Murphy D M 2009 *Chem. Phys. Lett.* **477** 340
- [45] Haerle R, Riedo E, Pasquarello A and Baldereschi A 2001 *Phys. Rev. B* **65** 045101
- [46] Sakthivel S and Kisch H 2003 *Angew. Chem. Int. Ed.* **42** 4908
- [47] Gu D, Lu Y, Yang B C and Hu Y D 2008 *Chem. Commun.* **21** 2453
- [48] Tauc J, Grigorovici R and Vancu A 1966 *Phys. Stat. Sol.(b)* **15** 627